doi: 10.29382/eqs-2020-0239-01

Measuring PmP travel times using teleseismic S-wave waveform data*

Lupei Zhu✉ and Yuchen Liu

Department of Earth and Atmospheric Sciences, *Saint Louis University*, *St. Louis*, *MO* 63108, *USA*

Abstract Joint inversion for crustal velocity structure using only surface wave dispersion and receiver function data often suffers the non-unique solution problem due to lack of P wave velocity constraint in the data. Here we developed a method for measuring PmP travel time using teleseismic S wave waveform. The major improvement by this method over the previous one-layer-crust search method is its use of a more realistic multi-layer-crust (MLC) velocity model in the study region based on available information. Numerical tests show that compared with the previous search method the MLC search method is faster and more reliable and accurate. One limit of the MLC search method is the requirement of a multi-layer background model, thus this method might not be applicable in regions where the velocity structure is unknown. Nevertheless, our numerical tests show that the MLC search method is robust in the sense that small deviations of the background model from the true velocity model do not influence the results severely. We applied the MLC search method to data from a temporary linear array across the Wabash Valley Seismic Zone in the central USA. We obtained 157 PmP travel-time measurements that show lateral crustal structure variation in the region. The measurements provide additional constraints in joint inversion for crustal velocity structure in this seismically active region.

Keywords: PmP travel time; teleseismic S-wave waveform; crustal structure; Wabash Valley Seismic Zone

1 Introduction

Joint inversion of surface wave dispersion and teleseismic receiver function (RF) data has become popular in obtaining crustal velocity structures recently. RFs can be readily computed for every single three-component broad-band station and surface wave dispersion at the station site can be obtained by ambient noise tomography (ANT). These two types of observations, one sensitive to velocity jumps and the other sensitive to averaged velocity, help to reduce the trade-off between the velocity and interface depth and therefore to reduce the non-uniqueness of the inversion solution. However, both datasets are mostly sensitive to the S-wave velocity structure and lack of P-wave velocity constraint. On the other hand, seismic interface depths based on the RF data depend strongly on the v_P/v_S ratio of the media. If the P-wave velocities are not constrained, neither are the interface depths and S-wave velocities of the inversion results.

Crustal P-wave velocities are often obtained through travel time tomography using local earthquakes (e.g. Lei et al., 2008; Wang et al., 2018), but the coverage depends on the seismicity level and events distribution in the region. The deep seismic sounding (DSS) method uses artificial sources and has high resolution power, but can only cover a small region and is expensive. It is desirable to develop station-based techniques like the RF and ANT methods to obtain P-wave travel time data that are independent of earthquake sources. One solution is to use teleseismic S-wave waveform records. When an upward-traveling S-wave from a teleseismic event encounters the free surface, part of its energy will be reflected back as a P wave. The P wave will be reflected again by the Moho and be recorded by stations at the surface. This phase is called SsPmp following the naming convention of Storchak et al. (2003) (Figure 1). The SsPmp phase has been observed at both teleseismic (e.g. Langston, 1996) and regional distances (e.g. Zhu et al., 1997; Poli et al., 2012). If the ray parameter of the incident S wave exceeds a certain value dependent on the mantle P velocity beneath the Moho, the Moho reflection becomes post-critical and the SsPmp amplitude will be comparable to that of the direct S wave. The arrival time difference between the SsPmp and direct S phase is the PmP travel time (t_{PmP}) (with the horizontal distance x's contribution px subtracted, where p is the horizontal slowness of the incident S wave) as if the source

* **Received** 12 July 2020; **accepted in revised form** 14 October 2020; **published** 21 December 2020.

✉ **Corresponding author. e-mail**: lupei.zhu@slu.edu

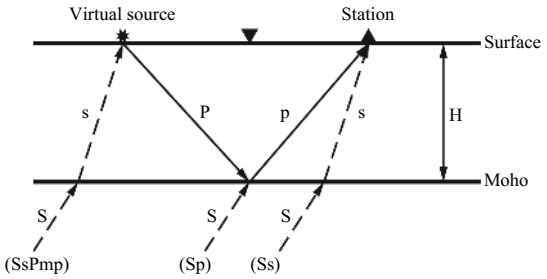

Figure 1 Ray paths of teleseismic Ss, Sp, and SsPmp phases, from Luo et al. (2018).

is at the surface (Figure 1). This technique has been referred as the virtual deep seismic sounding (VDSS) method (Tseng et al., 2009; Yu et al., 2012; 2016).

Extracting t_{PmP} from teleseismic S wave waveform is not easy due to a phase shift to the SsPmp waveform after the post-critical reflection at the Moho. Simply cross-correlating waveforms of S and SsPmp phases would not work. Luo et al. (2018) developed a deconvolution and grid-search technique to measure t_{PmP}. One shortcoming of the technique is that it uses a one-layer crustal model. The model is likely oversimplified and does not represent the real crustal structure. Errors in the model response would be mapped into the results. In this study, we improved the method by using a multi-layer-crust (MLC) model that can be obtained from available information in the study region. We will first describe how t_{PmP} can be obtained from teleseismic S-wave waveform data. We then used numerical tests to verify the MLC search method and to compare its results with those of the previous method. We will apply the method to a dense linear array in the Wabash Valley Seismic Zone (WVSZ) in the USA. The advantages and the limits of the MLC search method are discussed in the end.

2 Method

The observed teleseismic waveform $u(t)$ can be expressed as a convolution of the effective source time function (STF) $S(t)$ and the response $R(t)$ of the crustal structure beneath the station:

$$u(t) = S(t) \otimes R(t). \quad (1)$$

Luo et al. (2018) simplified the crust as a one layer of thickness H and P wave velocity v_P. For given values of H and v_P, $R(t)$ is calculated using the frequency-wavenumber (FK) integration method (Zhu and Rivera, 2002). The STF is then estimated by deconvolving $R(t)$ from $u(t)$, and the misfit between the observed and predicted waveforms is calculated using the L_2 norm square of the difference:

$$E = \left\| u^{obs} - u^{pre} \right\|^2. \quad (2)$$

The procedure is repeated using different H and v_P, and their optimal values are found from the minimum of E. Finally, the best estimation of t_{PmP} is calculated using

$$t_{PmP} = 2\sum_{i=1}^{n} h_i \sqrt{\frac{1}{V_{Pi}^2} - p^2}, \quad (3)$$

where n is the total number of crustal layers, h_i is the thickness of the i-th layer. Since a one-layer crustal model is used in the procedure, we referred this method as the one-layer-crust search method.

We modified the above method by using a more realistic multiple-layered background velocity model. The new method is illustrated in Figure 2. By changing the Moho depth H of the background model, we generated a series of trial velocity models. The optimal Moho depth is obtained by searching for the minimum misfit between the observed and predicted waveforms. Its uncertainty σ_H is estimated using the curvature of the E at the minimum (e.g. Menke, 1989),

$$\sigma_H^2 = \frac{2E_{min}}{N-1}\left[\frac{\partial^2 E}{\partial H^2}\right]^{-1}, \quad (4)$$

where N is the total number of independent data points. The corresponding t_{PmP} and uncertainty are then calculated using Equation (3). We called this method the MLC search method.

3 Numerical tests

We conducted three numerical tests to show the improvements of the MLC search method over the previous search method. In the first two tests, we compared the performance of the two methods using noise-free and noise-added waveform data, respectively. In the third test, we demonstrated the robustness of the MLC search method by using different background models.

The true model we used for all the tests is a four-layer model consisting of a sedimentary layer, the upper crust, the lower crust, and the mantle (Figure 2a). The v_P/v_S ratio was fixed to 1.78 for all the layers. The impulse response of the model was generated using the FK method with a ray parameter of 0.13 s/km. We then convolved it with a triangle STF of 3 s wide and applied a Butterworth bandpass filter with corner frequencies of 0.08 Hz and 1 Hz to obtain the noise-free waveforms (Figure 2b).

In the multi-layer-crust search, we used a five-layer model as the background model (Figure 3). We searched for the optimal thickness of the layer above the Moho from 2 to 36 km at an increment of 2 km (Figure 3). The best

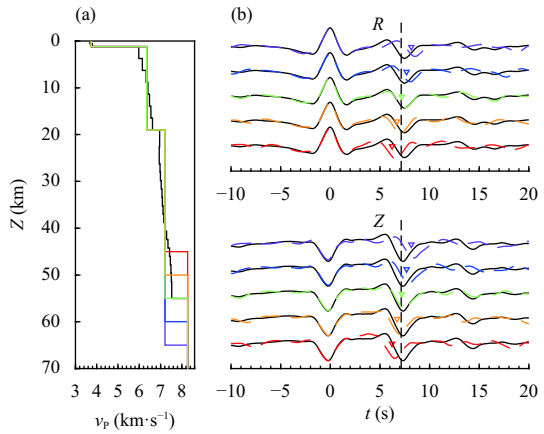

Figure 2 The multi-layer-crust search method for measuring t_{PmP}. (a) Black lines represent the true model and colored ones are background models of different Moho depths. (b) Radial (R) and vertical (Z) components of observed teleseismic S-wave waveform (black) and predictions by different background models. The triangle shows the t_{PmP} prediction by the corresponding model and the black dashed line represents the true t_{PmP}

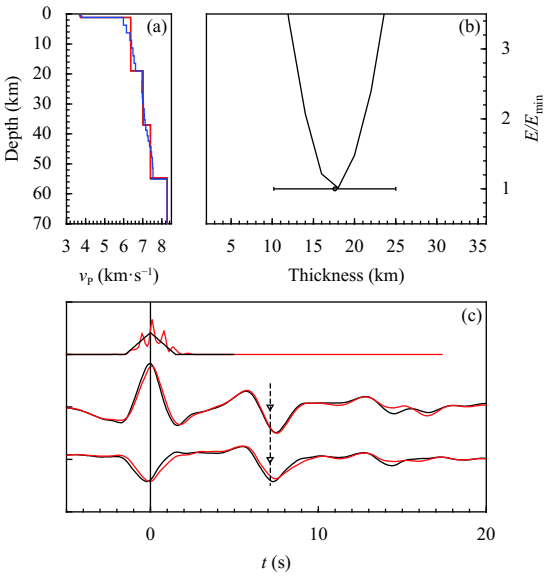

Figure 3 Multi-layer-crust search results using noise-free waveform data. (a) The true P-wave velocity model (blue), the background model (black), and the obtained model (red). (b) Waveform misfit as a function of the thickness of the layer above the Moho. The circle with error bar represents the best thickness obtained. (c) From the top to bottom, the true (black) and estimated (red) STF, observed (black) and predicted (red) radial (R) and vertical (Z) waveforms. The triangle indicates the obtained t_{PmP} and the dashed line indicates the true t_{PmP}

Moho depth was found to be 53.6±1.1 km, very close to the true value of 55.0 km. The obtained t_{PmP} is (7.13±0.08) s, which is only 0.01 s less than the true value of 7.14 s. The predicted waveforms match the observed waveforms very well and the estimated STF is close to the true STF (Figure 3).

In the one-layer-crust search, the mantle P- and S-wave velocities of the background model were fixed to the true values. The crustal layer P-wave velocity and thickness were searched from 6.3 km/s to 7.3 km/s at an increment of 0.1 km/s and from 40 km to 70 km at an increment of 2 km, respectively (Figure 4). The crustal S-wave velocity was obtained using the v_P/v_S ratio in the true model. The best Moho depth and crustal P-wave velocity from this method are (56.2±1.3) km and (6.99±0.03) km/s, respectively. The obtained t_{PmP} is (6.69±0.16) s, which is less than the true value by 0.45 s. The predicted waveforms do not match well with the observed waveforms. There is a clear time shift between the observed and predicted vertical-component waveforms (Figure 4).

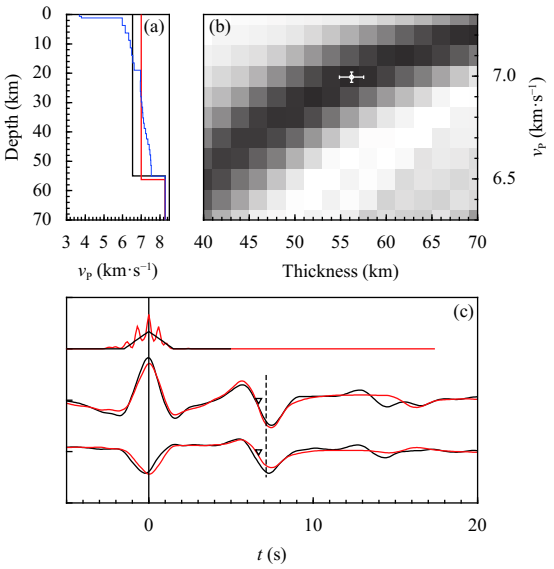

Figure 4 One-layer-crust search results using noise-free waveform data, see Figure 3 caption for explanation

We then repeated the above tests but added 10% random noise to the waveform "data". The optimal Moho depth from the MLC search method is (56.7±2.4) km (Figure 5) which differs from the true value slightly, more than the result using the noise-free waveforms. The obtained t_{PmP} changes from 7.13 s to 7.35 s and its uncertainty increases from 0.08 s to 0.18 s. The waveform fits to the R- and Z-component waveforms are still good, and the estimated STF is close to the true STF (Figure 5). The optimal Moho depth and crustal P-wave velocity from the one-layer-crust search are (41.9±1.3) km and (6.52±0.06) km/s, respectively (Figure 6). The obtained t_{PmP} is (6.81±0.22) s, the worst in all cases when comparing the true value.

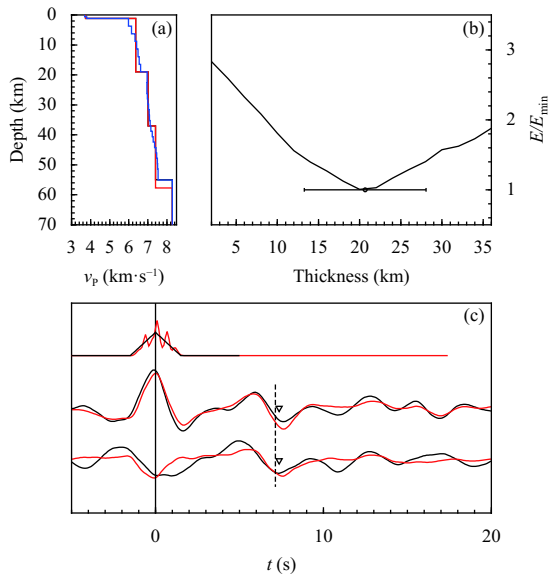

Figure 5 Multi-layer-crust search results using noise-added waveform data. (a) The true P-wave velocity model (blue), the background model (black), and the obtained model (red). (b) Waveform misfit as a function of the thickness of the layer above the Moho. The circle with error bar represents the best thickness obtained. (c) From the top to bottom, the true (black) and estimated (red) STF, observed (black) and predicted (red) radial (R) and vertical (Z) waveforms. The triangle indicates the obtained tPmP and the dashed line indicates the true t_{PmP}

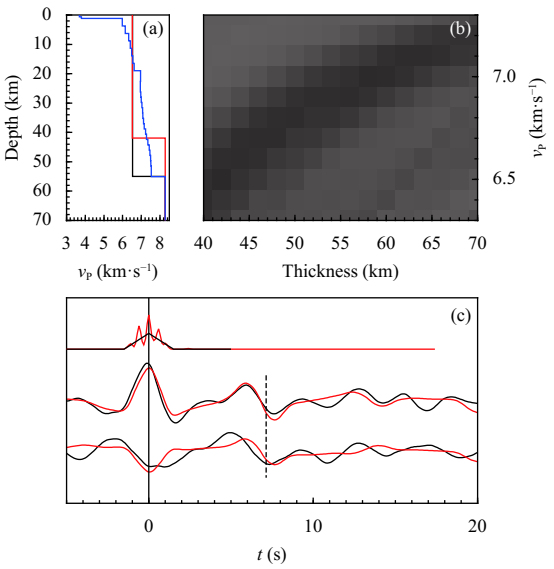

Figure 6 One-layer-crust search results using noise-added waveform data, see Figure 4 caption for explanation

Our MLC search method requires a background velocity model that is an approximation of the true velocity structure. The influences of the background model on the t_{PmP} measurements need to be investigated. In the third test, we used 100 different background velocity models by randomly perturbing the background model above (Figure 7a). The t_{PmP}'s of these background models have a wide distribution ranging between 6.74 s and 7.71 s (Figure 7b). After the search, the obtained t_{PmP} values concentrate around the true value. The mean of the 100 obtained t_{PmP} values is 7.15 s, which is very close to the true value, with a small standard deviation of 0.04 s.

4 Application to the WVSZ array data

We applied the MLC search method to waveform data of a linear temporary array across the WVSZ (Figure 8). More than 2,000 teleseismic events were recorded during

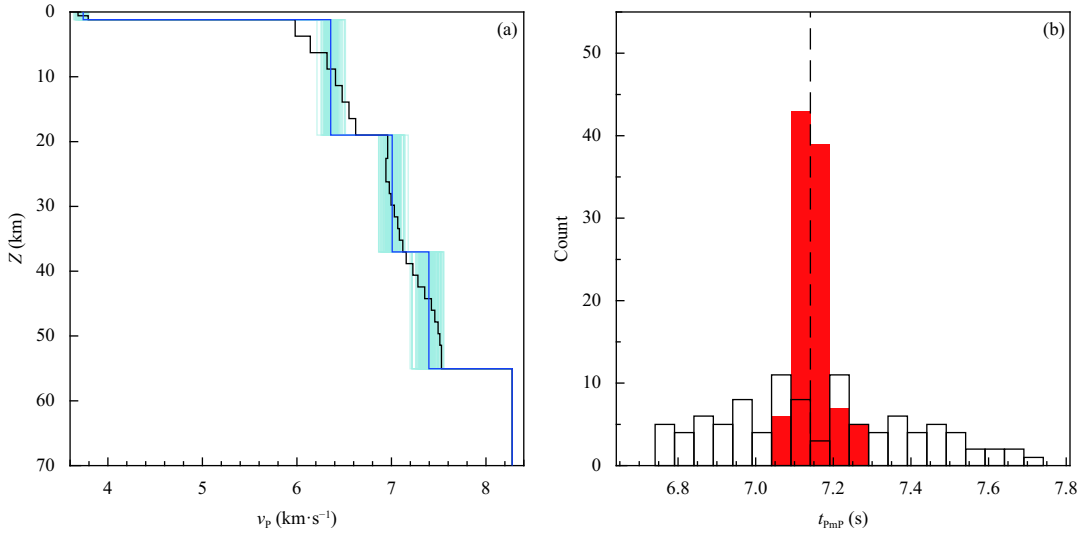

Figure 7 (a) The true model (black) and randomly generated background models (blue). (b) Histograms of t_{PmP}'s before (black) and after (red) searching with different models in (a). The dashed line is the true t_{PmP}

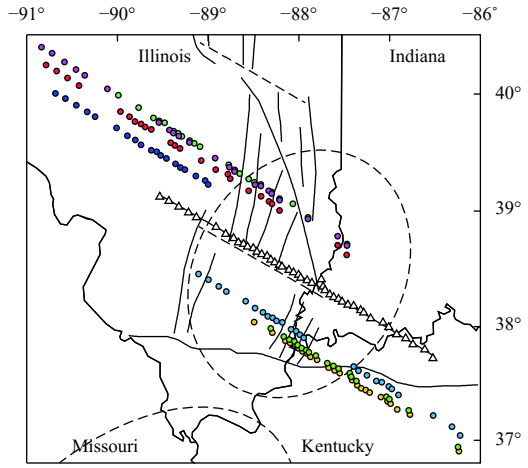

Figure 8 Triangles represent 48 temporary broadband seismic stations deployed across the Wabash Valley Seismic Zone (the dashed line ellipsis) in southern Illinois-Indiana, USA. Heavy black lines are mapped faults in the region. Color-coded circles represent 157 Moho reflection points of SsPmp phase from 7 teleseismic events used in this study

the two-year deployment. We used several criteria to select events, namely: ① the event had more than five station recordings; ② the event's back-azimuth was within 15° of the linear array direction; ③ the epicentral distance was between 35° and 65°; ④ the magnitude was between 5.0 and 7.0; and ⑤ the focal depth was greater than 50 km. Events with a back-azimuth along the array direction had PmP reflection points close to the array. The epicentral distance constraint ensured that the S-wave ray parameter reached the critical PmP reflection threshold. Events with magnitudes of 5–7 had strong S phases, while the source time functions were not too complicated. We selected only deep events so that the SsPmp phase would not be contaminated by the depth phases. We also inspected the waveforms and rejected those of low signal-to-noise ratios. Finally, seven events and a total of 157 waveform records with clear S arrivals were selected (Table 1).

Table 1 Origin times and locations of events used

Date	Time	Lat.(°)	Lon.(°)	Dep(km)	M	p (s/km)
2014-08-24	23:21:45	–14.60	–73.57	101	6.8	0.120
2014-08-25	14:31:37	–16.12	–73.11	62	5.5	0.119
2014-09-25	17:51:17	61.94	–151.82	109	6.2	0.130
2015-03-23	04:51:38	–18.35	–69.17	130	6.4	0.116
2015-05-29	07:00:09	56.59	–156.43	73	6.7	0.128
2015-06-24	22:32:21	61.66	–151.96	114	5.7	0.130
2015-07-29	02:35:59	59.89	–153.20	119	6.3	0.129

We cut three-component waveforms from the continuous recordings using a time window of 50 s before and 50 s after the theoretical S arrival time. We applied a Butterworth bandpass filter with corner frequencies of 0.08 Hz and 1 Hz to the waveforms to eliminate long period and high frequency noise. We then rotated the horizontal components to the radial and transverse directions. Figure 9 shows the R- and Z-component waveforms of event 2015-07-29 02:35:59.

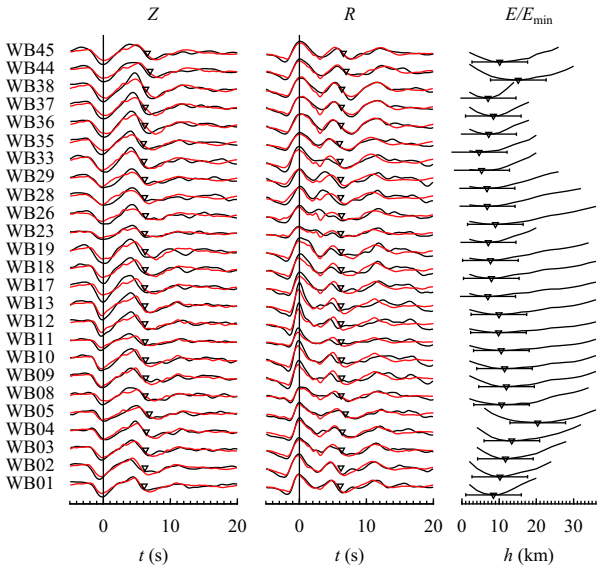

Figure 9 Black traces are observed radial (R), vertical (Z) S-wave waveforms, and normalized misfit (E/Emin) for event 20150729023559. Red traces are predicted waveforms from the multi-layer-crust search method. Triangles show the t_{PmP} measurements and optimal thickness h of the layer above the Moho

The background model used for measuring t_{PmP} was obtained based on a joint inversion study by Aziz Zanjani et al. (2019) who obtained 152 1-D S-wave velocity models along the linear array. We used a six-layer background velocity model by averaging those 1-D models (Figure 10). The v_P/v_S ratios of all layers were fixed to 1.78. We searched the Moho depth from 36 km to 70 km with an increment of 2 km. Figure 10 shows the search results at station WB01 for the example event. The predicted waveforms of all available stations are plotted in Figure 9. The waveform fiting to the observed waveforms are generally good and the t_{PmP} measurements are consistent and show coherent variation.

We applied the MLC search method to all seven events and obtained a total of 157 t_{PmP} measurements. Since t_{PmP} is a function of ray parameter p, we corrected the measurements to a common ray parameter of 0.10 s/km using the background model and Equation (3). The corrected t_{PmP} values were assigned to their PmP reflection points and were plotted as a function of the reflection position

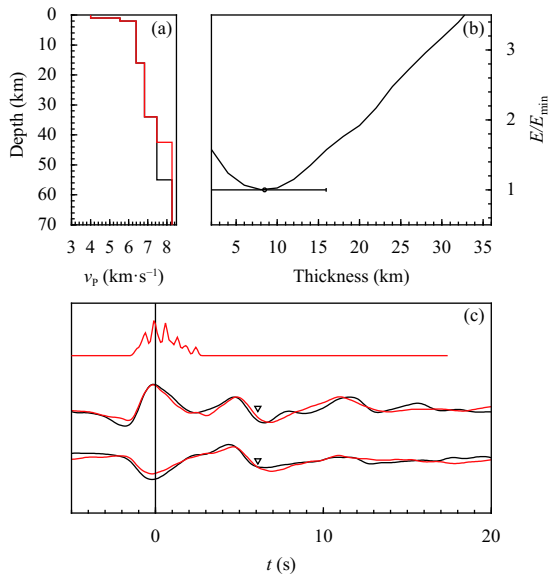

Figure 10 Multi-layer-crust search results at station WB01 for event 20150729023559, see Figure 3 caption for explanation.

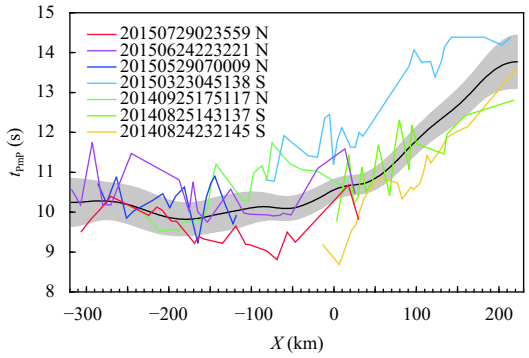

Figure 11 Color lines show variations of t_{PmP} measurements from individual events as a function of the reflection point position along the linear array from NW to SE (the PmP reflection points are shown in Figure 8). The black curve and gray area are smoothly interpolated t_{PmP} times and their uncertainties, respectively

along the linear array from NW to SE (Figure 11). Overall, the t_{PmP} value varies between 8.7 and 14.4 s and the measurement standard deviation varies from 0.2 to 2.3 s. Around any given reflection point, the t_{PmP} values from different events differ by 0.2 to 2.0 s, due to waveform noise and 3-D crustal structural variation. Nevertheless, the t_{PmP} measurements of all seven events show a consistent trend of lower values in the northwestern side of the array and higher values in the southeastern side (Figure 11). Because the linear array direction is roughly perpendicular to the axis of Wabash Valley (Figure 8), we simplified the crustal structure beneath the array as 2-D and used a least-squares inversion with smoothness constraint to obtain a smoothly varying t_{PmP} as a function of the PmP reflection point position along the linear array (Figure 11). The smoothed t_{PmP} values along with their standard deviations were used in a joint inversion with surface wave dispersion and RF data to obtain a 2-D image of crustal structure across the WVSZ that shows a relatively flat Moho of 51–55 km deep and a strong variation of crustal v_P/v_S ratio from 1.69 to 1.90 (Liu and Zhu, 2021).

5 Discussion and conclusions

The major improvement offered by our MLC search method over the previous search method is the use of a more realistic background model that better represents the structure of the study region. It is also one order of magnitude faster than the previous search method since it only searches for the crustal thickness H instead of both H and v_P in the latter case. The numerical tests show that our MLC search method is more accurate than the previous search method for measuring t_{PmP} using teleseismic S-wave waveforms. Test one using noise-free data shows that the difference between true and measured t_{PmP} from the MLC search method is 0.01 s, only ~0.1% of the true t_{PmP} value. On the other hand, the difference from the one-layer-crust search method is 0.45 s, which is 45 times larger than that from the MLC search method. With noise added, the MLC search method still performed well and gave a t_{PmP} measurement of 7.35 s, which is ~2.9% larger than the true t_{PmP}. In contrast, the t_{PmP} measurement from the one-layer-crust search method is lower than the true t_{PmP} value by ~8.7%.

The MLC search method is also more reliable than the previous search method. Numerical tests indicate that the MLC search method results have a lower uncertainty than the previous search method results using both noise-free and noise-added waveforms. The uncertainty of measured t_{PmP} from the MLC search method using noise-free data is 0.08 s, which is ~50% lower than that from the previous search method (0.16 s). With noise added, t_{PmP} uncertainties in both the MLC and previous search methods increase, but the uncertainty in the MLC search method is still ~22% lower than that in the previous search method.

The MLC search method requires a multi-layer background velocity model of the study area. In regions where the velocity structure has not been thoroughly investigated, a simple crustal model or global model has to be used. In numerical test three, we used different background models in the MLC search method. The measured t_{PmP} values are narrowly centered at the true t_{PmP} value, with a standard deviation of ~0.6% of the true value.

The results suggest that the MLC search method is robust and small deviations of the background model from the true velocity model do not have a large influence on the t_{PmP} measurements.

In summary, we developed the MLC search method for measuring t_{PmP} using teleseismic S-wave waveform. The major improvement by the MLC search method over the previous search method is its use of a more realistic background velocity model in the study region based on available information. Numerical tests show that compared with the previous search method the MLC search method is faster and more reliable and accurate. One limit of the MLC search method is the requirement of a multi-layer background model, thus this method might not be applicable in regions where the velocity structure is unknown. Nevertheless, our numerical tests show that the MLC search method is robust in the sense that small deviations of the background model from the true velocity model do not influence the results severely. We applied the MLC search method to data from a temporary linear array across the Wabash Valley Seismic Zone in the central USA. We obtained 157 t_{PmP} measurements that show lateral crustal structure variation in the region. The measurements provide additional constraints in joint inversion for crustal velocity structure in this seismically active region.

Acknowledgments

The study was supported by US NSF grants EAR-1249701 and EAR-1661519. We are grateful to Linda Warren, Bob Herrmann, and two anonymous reviewers whose comments helped us to improve the manuscript. Waveform data of the 2014–2016 Wabash Valley Seismic Recording Experiment (network code 6E) have been archived at the IRIS DMC and are available for downloading.

References

Aziz Zanjani A, Zhu L, Herrmann RB, Liu Y and Conder JA (2019) Crustal structure beneath the Wabash Valley Seismic Zone from the joint inversion of receiver functions and surface-wave dispersion: implications for continental rifts and intraplate seismicity. J Geophys Res **124**: 7028–7039

Langston CA (1996) The SsPmp phase in regional wave propagation. Bull Seismol Soc Amer **86**(1A): 133–143

Lei J, Xie F, Lan C, Xing C and Ma S (2008) Seismic images under the Beijing region inferred from P and PmP data. Phys Earth Planet Inter **168**: 134–146

Liu Y and Zhu L (2021) Joint inversion for crustal seismic *S*- and *P*-wave velocity structures with interfaces. Geophys J Int doi:10.1093/gji/ggab092

Luo S, Zhu L, Huang R, Luo Y, Jiang X and Hua Y (2018) Determination of crustal thickness and velocities by using receiver functions and PmP travel times. Geophys J Int **216**: 1304–1312

Menke W (1989) Geophysical Data Analysis: Discrete Inverse Theory. San Diego, Academic Press, p.66

Poli P, Pedersen HA, Campillo M and the POLENET/LAPNET Working Group (2012) Emergence of body waves from cross-correlation of short period seismic noise. Geophys J Int **188**: 549–558

Storchak DA, Schweitzer J and Bormann P (2003) The IASPEI standard seismic phase list. Seismol Res Lett **74**: 761–772

Tseng T-L, Chen W-P and Nowack RL (2009) Northward thinning of Tibetan crust revealed by virtual seismic profiles. Geophys Res Lett **36**: L24304

Wang H, Zhao D, Huang Z, Xu M, Wang L, Nishizono Y and Inakura H (2018) Crustal tomography of the 2016 Kumamoto earthquake area in West Japan using P and PmP data. Geophys J Int **214**: 1151–1163

Yu C, Chen W-P and van der Hilst RD (2016) Constraints on residual topography and crustal properties in the western United States from virtual deep seismic sounding. J Geophys Res **121**: 5917–5930

Yu C-Q, Chen W-P, Ning J-Y, Tao K, Tseng T-L, Fang X-D, Chen YJ and van der Hilst RD (2012) Thick crust beneath the Ordos plateau: Implications for instability of the North China craton. Earth Planet Sci Lett **357-358**: 366–375

Zhu L and Rivera LA (2002) A note on the dynamic and static displacements from a point source in multilayered media. Geophys J Int **148**: 619–627

Zhu L, Helmberger DV, Saikia CK and Woods BB (1997) Regional waveform calibration in the Pamir-Hindu Kush region. J Geophys Res **102**: 22799–22813